

Seismogram synthesis for radially layered media using the generalized reflection/transmission coefficients method: Theory and applications to acoustic logging

Xiaofei Chen*, Youli Quan**, and Jerry M. Harris**

ABSTRACT

A new method based on generalized reflection and transmission coefficients is proposed to calculate the synthetic seismograms in radially multilayered media. This method can be used to efficiently simulate full waveform acoustic logs and crosswell seismic profiles in situations where we need to consider borehole effects. The new formulation is tested by comparing our numerical results with previous available work and shows excellent agreement. Because of the use of the normalized Hankel functions and the normalization factors, this new algorithm for computing seismograms is stable numerically even for high-frequency problems. To show the applicability of this new approach to full waveform sonic logging, we apply it to investigate the effects of complex invaded zones on the geometrical spreading and attenuation estimation for P-waves. We find that a damaged zone (its velocity is slower than the unperturbed formation velocity) exhibits a convergence effect on the P-waves, and a flushed zone (velocity is faster than the unperturbed formation velocity) exhibits a divergence effect on the P-waves.

INTRODUCTION

Sonic logging in cased boreholes is useful for evaluating the quality of the cement job. Also, effort is being made to measure the formation properties from full waveform sonic logs run in cased boreholes. A cased borehole and any near borehole alteration, e.g., mudcake and invaded zones, can be modeled as a radially layered medium. Study of elastic waves in a radially layered medium is useful for understanding and interpreting full waveform sonic logs. Tubman et al. (1984) used the Thomson-Haskell method to study this problem. In this study,

we propose an alternative approach, the generalized reflection and transmission (R/T) coefficients method, to solve this problem. The generalized R/T coefficients method is used widely in modeling the elastic waves in vertically layered media because of its computational stability and efficiency over the Thomson-Haskell method, especially for high-frequency problems (e.g., Luco and Apsel, 1983; Kennett, 1983; Chen, 1993). Yao and Zheng (1985) derived a set of formulas for computing synthetic seismograms in a radially layered borehole environment using the generalized R/T coefficients method, but they did not conduct numerical tests to check their formulation. We derive a set of alternative formulations that are more stable and efficient than the previous methods for numerical computation. First, we introduce the concepts of modified and generalized reflection and transmission matrices for the radially layered media and derive a recursive scheme to calculate them. Then, we determine wavefields using the R/T matrices. To check the formulation, we compare our calculated results with that of Tubman et al. (1984) for a four-layer cased borehole model and those of Baker (1984) for borehole models with invaded zones. For applications to acoustic logging, we study the effects of invaded zones on geometrical spreading and attenuation measurement of the P-waves.

GOVERNING EQUATIONS AND THEIR GENERAL SOLUTIONS

The radially multilayered model considered in this study is shown in Figure 1. The first layer ($r < r^{(1)}$) is fluid. A point source is located at $r = 0$ and $z = 0$. For this radially symmetrical problem, there are only P - and SV -waves, i.e., the displacement can be written as

$$\mathbf{u} = \nabla\phi + \nabla \times (\mathbf{e}_\theta\psi), \quad (1)$$

where ϕ and ψ are P-wave and S-wave potentials, respectively. Substituting equation (1) into the elastodynamic equation in the frequency domain, we obtain

Presented at the 64th Annual International Meeting, Society of Exploration Geophysicists. Manuscript received by the Editor January 23, 1995; revised manuscript received August 25, 1995.

*Department of Earth Sciences, University of Southern California, Los Angeles, California 90089.

**Department of Geophysics, Stanford University, Stanford, California 94305.

© 1996 Society of Exploration Geophysicists. All rights reserved.

$$\frac{\partial^2 \phi^{(j)}}{\partial r^2} + \frac{1}{r} \frac{\partial \phi^{(j)}}{\partial r} + \frac{\partial^2 \phi^{(j)}}{\partial z^2} + k_\alpha^{(j)2} \phi^{(j)} = F(\omega) \frac{\delta(r)\delta(z)}{2\pi r}, \quad (2a)$$

$$\frac{\partial^2 \psi^{(j)}}{\partial r^2} + \frac{1}{r} \frac{\partial \psi^{(j)}}{\partial r} - \frac{\psi^{(j)}}{r^2} + \frac{\partial^2 \psi^{(j)}}{\partial z^2} + k_\beta^{(j)2} \psi^{(j)} = 0, \quad (2b)$$

for $r^{(j-1)} < r < r^{(j)}$, where j denotes the layer index and $j = 1, 2, \dots, N$ (define $r^{(0)} = 0$). In equation (1), $k_\alpha^{(j)} = \omega/\alpha^{(j)}$, $k_\beta^{(j)} = \omega/\beta^{(j)}$, $F(\omega)$ is the source spectrum, and α and β are the velocities of the P-wave and S-wave, respectively. In the $k - \omega$ domain, the solutions of equations (2a) and (2b) are

$$\begin{aligned} \bar{\phi}_k^{(j)}(r) &= c_{p-}^{(j)} e^{iv_\alpha^{(j)}(r^{(j)}-r)} \bar{H}_0^{(2)}(v_\alpha^{(j)}r) \\ &\quad + c_{p+}^{(j)} e^{iv_\alpha^{(j)}(r-r^{(j-1)})} \bar{H}_0^{(1)}(v_\alpha^{(j)}r), \end{aligned} \quad (3a)$$

$$\bar{\psi}_k^{(j)}(r) = c_{s-}^{(j)} e^{iv_\beta^{(j)}(r^{(j)}-r)} \bar{H}_1^{(2)}(v_\beta^{(j)}r) + c_{s+}^{(j)} e^{iv_\beta^{(j)}(r-r^{(j-1)})} \bar{H}_1^{(1)}(v_\beta^{(j)}r), \quad (3b)$$

where $v_\alpha^{(j)} = \sqrt{k_\alpha^{(j)2} - k^2}$, $\text{Im}\{v_\alpha^{(j)}\} > 0$, $v_\beta^{(j)} = \sqrt{k_\beta^{(j)2} - k^2}$, $\text{Im}\{v_\beta^{(j)}\} > 0$, and $j = 2, 3, \dots, N$. In the outermost layer ($j = N + 1$), there exists only outward-going waves, i.e.,

$$\bar{\phi}_k^{(N+1)}(r) = c_{p+}^{(N+1)} e^{iv_\alpha^{(N+1)}(r-r^{(N)})} \bar{H}_0^{(1)}(v_\alpha^{(N+1)}r), \quad (4a)$$

$$\bar{\psi}_k^{(N+1)}(r) = c_{s+}^{(N+1)} e^{iv_\beta^{(N+1)}(r-r^{(N)})} \bar{H}_1^{(1)}(v_\beta^{(N+1)}r), \quad (4b)$$

where $v_\alpha^{(N+1)} = \sqrt{k_\alpha^{(N+1)2} - k^2}$, $\text{Im}\{v_\alpha^{(N+1)}\} > 0$, $v_\beta^{(N+1)} = \sqrt{k_\beta^{(N+1)2} - k^2}$ and $\text{Im}\{v_\beta^{(N+1)}\} > 0$. Here, $\bar{H}_n^{(1)}(x) = e^{-ix} H_n^{(1)}(x)$ and $\bar{H}_n^{(2)}(x) = e^{ix} H_n^{(2)}(x)$ are the first and second kind normalized Hankel functions of n th order, respectively. $c_{p-}^{(j)}$, $c_{p+}^{(j)}$, $c_{s-}^{(j)}$, and $c_{s+}^{(j)}$ are unknowns, where “+” refers to outgoing waves and “-” refers to incoming waves. It should be emphasized that instead of the ordinary Hankel functions [$H_n^{(1)}(x)$ and $H_n^{(2)}(x)$] we use the normalized Hankel functions [$\bar{H}_n^{(1)}(x)$ and $\bar{H}_n^{(2)}(x)$], whose asymptotic behavior for a large imaginary argument is less oscillatory, to express the solutions. Thus, our algorithm is stable numerically even for high-frequency problem. We shall discuss this further in a later section. For $j = 1$, in the fluid-filled borehole, we have

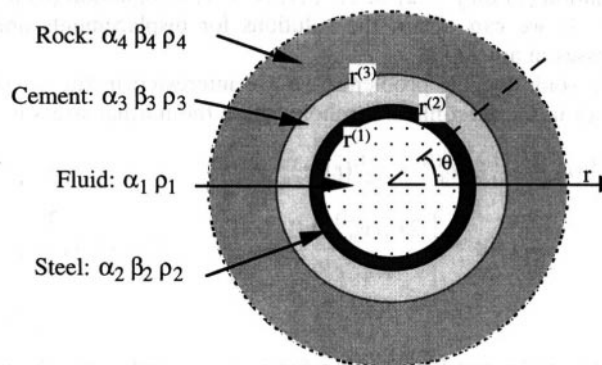


FIG. 1. A radially multilayered model.

$$\begin{aligned} \bar{\phi}_k^{(1)}(r) &= c J_0^{(1)}(r) + s_+ H_0^{(1)}(v_\alpha^{(1)}r) \\ &= c_{p-}^{(1)} e^{iv_\alpha^{(1)}(r^{(1)}-r)} \bar{H}_0^{(2)}(v_\alpha^{(1)}r) \\ &\quad + (c_{p+}^{(1)} + s_+) e^{iv_\alpha^{(1)}r} \bar{H}_0^{(1)}(v_\alpha^{(1)}r), \end{aligned} \quad (5)$$

where

$$c_{p+}^{(1)} = c_{p-}^{(1)} e^{iv_\alpha^{(1)}r^{(1)}} = \frac{c}{2}, \quad (6)$$

and

$$s_+ = -\frac{i}{4} F(\omega),$$

where J_0 is Bessel function of the first kind of order zero.

Using the above potential solutions, we obtain the radial and vertical components of the displacements ($\bar{u}_k^{(j)}$ and $\bar{v}_k^{(j)}$) and the stresses ($\bar{\sigma}_k^{(j)}$ and $\bar{\tau}_k^{(j)}$) in the cylindrical solid layers ($j > 1$), as

$$\begin{bmatrix} \bar{u}_k^{(j)}(r) \\ \bar{v}_k^{(j)}(r) \\ \bar{\sigma}_k^{(j)}(r) \\ \bar{\tau}_k^{(j)}(r) \end{bmatrix} = \begin{bmatrix} e_{11}^{(j)}(r) & e_{12}^{(j)}(r) & e_{13}^{(j)}(r) & e_{14}^{(j)}(r) \\ e_{21}^{(j)}(r) & e_{22}^{(j)}(r) & e_{23}^{(j)}(r) & e_{24}^{(j)}(r) \\ e_{31}^{(j)}(r) & e_{32}^{(j)}(r) & e_{33}^{(j)}(r) & e_{34}^{(j)}(r) \\ e_{41}^{(j)}(r) & e_{42}^{(j)}(r) & e_{43}^{(j)}(r) & e_{44}^{(j)}(r) \end{bmatrix} \begin{bmatrix} c_{p-}^{(j)} \\ c_{s-}^{(j)} \\ c_{p+}^{(j)} \\ c_{s+}^{(j)} \end{bmatrix}. \quad (7)$$

For the first layer (i.e., the liquid layer), we have

$$\begin{bmatrix} \bar{u}_k^{(1)}(r) \\ \bar{\sigma}_k^{(1)}(r) \end{bmatrix} = \begin{bmatrix} e_{11}^{(1)}(r) & e_{12}^{(1)}(r) \\ e_{21}^{(1)}(r) & e_{22}^{(1)}(r) \end{bmatrix} \begin{bmatrix} c_{p-}^{(1)} \\ c_{p+}^{(1)} + s_+ \end{bmatrix}, \quad (8)$$

where the explicit expressions of the elements $\{e_{nm}^{(j)}\}$ are given in the Appendix. To determine the unknown coefficients for each layer (i.e., $c_{p\pm}^{(j)}$ and $c_{s\pm}^{(j)}$), we need to impose the boundary conditions at each interface. For the first and second layers (liquid-solid boundary), the boundary conditions are

$$\begin{bmatrix} \bar{u}_k^{(1)}(r^{(1)}) \\ \bar{\sigma}_k^{(1)}(r^{(1)}) \end{bmatrix} = \begin{bmatrix} \bar{u}_k^{(2)}(r^{(1)}) \\ \bar{\sigma}_k^{(2)}(r^{(1)}) \end{bmatrix}, \quad (9)$$

and

$$0 = \bar{\tau}_k^{(2)}(r^{(1)}). \quad (10)$$

For the j th interface ($j = 2, 3, \dots, N$), which is a solid-solid boundary, the boundary conditions are

$$\begin{bmatrix} \bar{u}_k^{(j)}(r^{(j)}) \\ \bar{v}_k^{(j)}(r^{(j)}) \\ \bar{\sigma}_k^{(j)}(r^{(j)}) \\ \bar{\tau}_k^{(j)}(r^{(j)}) \end{bmatrix} = \begin{bmatrix} \bar{u}_k^{(j+1)}(r^{(j)}) \\ \bar{v}_k^{(j+1)}(r^{(j)}) \\ \bar{\sigma}_k^{(j+1)}(r^{(j)}) \\ \bar{\tau}_k^{(j+1)}(r^{(j)}) \end{bmatrix}. \quad (11)$$

R/T MATRICES AND SOLUTION SYNTHESIS

In the preceding section, we obtained the general solutions with unknowns, $c_{p\pm}^{(1)}$, and $c_{p\pm}^{(j)}$, $c_{s\pm}^{(j)}$, and $c_{s\pm}^{(j)}$ for $j = 2, 3, \dots, N + 1$. To effectively determine the unknowns for each layer, we introduce modified and generalized reflection and transmission (R/T) matrices, and derive their explicit expressions by using the above boundary conditions.

Modified R/T matrices

The modified R/T matrices, $\mathbf{R}_+^{(j)}$, $\mathbf{R}_-^{(j)}$, $\mathbf{T}_+^{(j)}$, and $\mathbf{T}_-^{(j)}$, for solid-solid interfaces are defined by the relations

$$\begin{cases} \mathbf{c}_-^{(j)} = \mathbf{R}_{+-}^{(j)} \mathbf{c}_+^{(j)} + \mathbf{T}_-^{(j)} \mathbf{c}_-^{(j+1)} \\ \mathbf{c}_+^{(j+1)} = \mathbf{T}_+^{(j)} \mathbf{c}_+^{(j)} + \mathbf{R}_{-+}^{(j)} \mathbf{c}_-^{(j+1)}, \end{cases} \text{ for } j = 2, 3, \dots, N, \quad (12a)$$

where $\mathbf{c}_\pm^{(j)} = [c_{p\pm}^{(j)}, c_{s\pm}^{(j)}]^T$, and the modified R/T matrices, $\mathbf{R}_{+-}^{(j)}$, $\mathbf{R}_{-+}^{(j)}$, $\mathbf{T}_+^{(j)}$ and $\mathbf{T}_-^{(j)}$, are 2 X 2 matrices. For the first interface (liquid-solid), the modified R/T matrices, $\mathbf{R}_{+-}^{(1)}$, $\mathbf{T}_+^{(1)}$ and $\mathbf{R}_{-+}^{(1)}$ are defined by

$$\begin{cases} \mathbf{c}_-^{(1)} = \mathbf{R}_{+-}^{(1)} (\mathbf{c}_+^{(1)} + s_+) + \mathbf{T}_-^{(1)} \mathbf{c}_-^{(2)} \\ \mathbf{c}_+^{(2)} = \mathbf{T}_+^{(1)} (\mathbf{c}_+^{(1)} + s_+) + \mathbf{R}_{-+}^{(1)} \mathbf{c}_-^{(2)}, \end{cases} \quad (12b)$$

where $\mathbf{c}_-^{(1)} = \mathbf{c}_-^{(1)} \mathbf{R}_{+-}^{(1)}$ is a scalar and $\mathbf{T}_+^{(1)}$, $\mathbf{T}_-^{(1)}$, and $\mathbf{R}_{-+}^{(1)}$ are 1 X 2, 2 X 1, and 2 X 2 matrices, respectively. Substituting equation (7) into equation (11), then comparing with equation (12a) we obtain

$$\begin{bmatrix} \mathbf{R}_{+-}^{(j)} & \mathbf{T}_-^{(j)} \\ \mathbf{T}_+^{(j)} & \mathbf{R}_{-+}^{(j)} \end{bmatrix} = \begin{bmatrix} e_{11}^{(j)}(r^{(j)}) & e_{12}^{(j)}(r^{(j)}) & -e_{13}^{(j+1)}(r^{(j)}) & -e_{14}^{(j+1)}(r^{(j)}) \\ e_{21}^{(j)}(r^{(j)}) & e_{22}^{(j)}(r^{(j)}) & -e_{23}^{(j+1)}(r^{(j)}) & -e_{24}^{(j+1)}(r^{(j)}) \\ e_{31}^{(j)}(r^{(j)}) & e_{32}^{(j)}(r^{(j)}) & -e_{33}^{(j+1)}(r^{(j)}) & -e_{34}^{(j+1)}(r^{(j)}) \\ e_{41}^{(j)}(r^{(j)}) & e_{42}^{(j)}(r^{(j)}) & -e_{43}^{(j+1)}(r^{(j)}) & -e_{44}^{(j+1)}(r^{(j)}) \end{bmatrix}^{-1} \times \begin{bmatrix} -e_{13}^{(j)}(r^{(j)}) & -e_{14}^{(j)}(r^{(j)}) & e_{11}^{(j+1)}(r^{(j)}) & e_{12}^{(j+1)}(r^{(j)}) \\ -e_{23}^{(j)}(r^{(j)}) & -e_{24}^{(j)}(r^{(j)}) & e_{21}^{(j+1)}(r^{(j)}) & e_{22}^{(j+1)}(r^{(j)}) \\ -e_{33}^{(j)}(r^{(j)}) & -e_{34}^{(j)}(r^{(j)}) & e_{31}^{(j+1)}(r^{(j)}) & e_{32}^{(j+1)}(r^{(j)}) \\ -e_{43}^{(j)}(r^{(j)}) & -e_{44}^{(j)}(r^{(j)}) & e_{41}^{(j+1)}(r^{(j)}) & e_{42}^{(j+1)}(r^{(j)}) \end{bmatrix}, \quad (13)$$

for $j = 2, 3, \dots, N$. Similarly, from equations (8), (9), (10), and (12b), we find

$$\begin{bmatrix} \mathbf{R}_{+-}^{(1)} & \mathbf{T}_-^{(1)} \\ \mathbf{T}_+^{(1)} & \mathbf{R}_{-+}^{(1)} \end{bmatrix} = \begin{bmatrix} e_{11}^{(1)}(r^{(1)}) & -e_{13}^{(2)}(r^{(1)}) & -e_{14}^{(2)}(r^{(1)}) \\ e_{21}^{(1)}(r^{(1)}) & -e_{33}^{(2)}(r^{(1)}) & -e_{34}^{(2)}(r^{(1)}) \\ 0 & -e_{43}^{(2)}(r^{(1)}) & -e_{44}^{(2)}(r^{(1)}) \end{bmatrix}^{-1} \times \begin{bmatrix} -e_{12}^{(1)}(r^{(1)}) & e_{11}^{(2)}(r^{(1)}) & e_{12}^{(2)}(r^{(1)}) \\ -e_{22}^{(1)}(r^{(1)}) & e_{31}^{(2)}(r^{(1)}) & e_{32}^{(2)}(r^{(1)}) \\ 0 & e_{41}^{(2)}(r^{(1)}) & e_{42}^{(2)}(r^{(1)}) \end{bmatrix}. \quad (14)$$

Equations (13) and (14) provide the formulas for computing the modified R/T matrices for each layer.

Generalized R/T matrices

The generalized R/T matrices, $\hat{\mathbf{R}}_{+-}^{(j)}$ and $\hat{\mathbf{T}}_+^{(j)}$, are defined by the following relations:

$$\begin{cases} \mathbf{c}_+^{(j+1)} = \hat{\mathbf{T}}_+^{(j)} \mathbf{c}_+^{(j)} \\ \mathbf{c}_-^{(j)} = \hat{\mathbf{R}}_{+-}^{(j)} \mathbf{c}_+^{(j)} \end{cases} \text{ for } j = 2, 3, \dots, N; \quad (15a)$$

and

$$\begin{cases} \mathbf{c}_+^{(2)} = \hat{\mathbf{T}}_+^{(1)} (\mathbf{c}_+^{(1)} + s_+) \\ \mathbf{c}_-^{(1)} = \hat{\mathbf{R}}_{+-}^{(1)} (\mathbf{c}_+^{(1)} + s_+). \end{cases} \quad (15b)$$

Substituting equation (15) into equation (12) and rearranging terms, we obtain a recursive relation

$$\begin{cases} \hat{\mathbf{T}}_+^{(j)} = [\mathbf{I} - \mathbf{R}_{-+}^{(j)} \hat{\mathbf{R}}_{+-}^{(j+1)}]^{-1} \mathbf{T}_+^{(j)} \\ \hat{\mathbf{R}}_{+-}^{(j)} = \mathbf{R}_{+-}^{(j)} + \mathbf{T}_-^{(j)} \hat{\mathbf{R}}_{+-}^{(j+1)} \hat{\mathbf{T}}_+^{(j)}, \end{cases} \text{ for } j = N, N-1, \dots, 2, 1, \quad (16)$$

where \mathbf{I} is the unit matrix, $\hat{\mathbf{R}}_{+-}^{(j)}$ and $\hat{\mathbf{T}}_+^{(j)}$ are 2 X 2 matrices for $j > 1$, $\hat{\mathbf{T}}_+^{(1)}$ is a 2 X 1 matrix, and $\hat{\mathbf{R}}_{+-}^{(1)} = \hat{\mathbf{R}}_{+-}^{(1)}$ is a scalar. In the out& most layer ($j = N + 1$), only outward-going waves exist, i.e., $\mathbf{c}_-^{(N+1)} = 0$. Therefore

$$\hat{\mathbf{R}}_{+-}^{(N+1)} = \mathbf{0}. \quad (17)$$

Equation (16) along with the initial condition given by equation (17) provides an efficient recursive scheme to calculate the generalized R/T matrices from the modified R/T matrices given in equations (13) and (14). Our formulations for computing the R/T matrices are numerically stable because of the use of the normalized Hankel functions and the normalization factors $e^{iv_{\alpha,\beta}^{(j)} r^{(j)}}$ and $e^{-iv_{\alpha,\beta}^{(j)} r^{(j)}}$ in the potential solutions.

Solution synthesis

Having the generalized R/T matrices, we can compute the unknowns $\mathbf{c}_\pm^{(j)}$ for any layer. Therefore, we can determine the displacements and stresses for any layer. From equations (6) and (15b) we obtain

$$\begin{cases} c_{p+}^{(1)} + s_+ = (1 - \hat{\mathbf{R}}_{+-}^{(1)} e^{iv_{\alpha}^{(1)} r^{(1)}})^{-1} s_+ \\ c_{p-}^{(1)} = \hat{\mathbf{R}}_{+-}^{(1)} (1 - \hat{\mathbf{R}}_{+-}^{(1)} e^{iv_{\alpha}^{(1)} r^{(1)}})^{-1} s_+. \end{cases} \quad (18a)$$

Then, from equation (15b) we calculate the coefficients $\mathbf{c}_\pm^{(j)}$ by following relations

$$\begin{cases} \mathbf{c}_+^{(j)} = \hat{\mathbf{T}}_+^{(j-1)} \hat{\mathbf{T}}_+^{(j-2)} \dots \hat{\mathbf{T}}_+^{(1)} (1 - \hat{\mathbf{R}}_{+-}^{(1)} e^{iv_{\alpha}^{(1)} r^{(1)}})^{-1} s_+ \\ \mathbf{c}_-^{(j)} = \hat{\mathbf{R}}_{+-}^{(j)} \mathbf{c}_+^{(j)} \end{cases}, \quad (18b)$$

where $j = 2, 3, \dots, N, N + 1$. Incorporating $\mathbf{c}_\pm^{(j)}$ into equation (7) for $j = 2, 3, \dots, N, N + 1$, or equation (8) for $j = 1$, we can obtain the solutions for displacements and stresses in any layer.

In sonic logging problems, we are interested in the stress waves in the fluid-filled borehole where the normal stress is

$$\begin{aligned} \bar{\sigma}_k^{(1)}(r) &= e_{21}^{(1)}(r) c_{p-}^{(1)} + e_{22}^{(1)}(r) (c_{p+}^{(1)} + s_+) \\ &= \lambda^{(1)} k_{\alpha}^{(1)2} \left[\frac{2J_0(v_{\alpha}^{(1)} r) e^{iv_{\alpha}^{(1)} r^{(1)}} \hat{\mathbf{R}}_{+-}^{(1)}}{\hat{\mathbf{R}}_{+-}^{(1)} e^{iv_{\alpha}^{(1)} r^{(1)}} - 1} - H_0^{(1)}(v_{\alpha}^{(1)} r) \right] s_+. \end{aligned} \quad (19)$$

By taking inverse Fourier transforms over k and ω , we obtain the final solution in the spatial and time domain as

$$\sigma^{(1)}(r, z, t) = \frac{\rho^{(1)}}{2} \int_{-\infty}^{+\infty} \omega^2 F(\omega) e^{-i\omega t} \times \left\{ \int_{-\infty}^{+\infty} i \frac{J_0(v_\alpha^{(1)} r) e^{i v_\alpha^{(1)} z} \hat{R}_{+-}^{(1)}}{1 - e^{i v_\alpha^{(1)} z} \hat{R}_{+-}^{(1)}} e^{ikz} dk + \frac{1}{R} e^{ik_\alpha^{(1)} R} \right\} d\omega, \quad (20)$$

where, $R = \sqrt{r^2 + z^2}$ and $\hat{R}_{+-}^{(1)}$ is the generalized reflection coefficient on the first interface (fluid-solid interface).

IMPLEMENTATION AND VERIFICATION TESTS

The discrete wavenumber technique (Bouchon and Aki, 1977) and fast Fourier transform (FFT) are used to evaluate numerically the $k - \omega$ integral in equation (20). To check the validity of our formulation, we compare our results with previous available work.

Cased borehole

The first example considered is a four-layer cased borehole model chosen from Tubman et al. (1984), (see Figure 1). The parameters of the model are listed in Table 1. The spectrum of source function is described by

$$F(\omega) = \frac{1}{\omega^2} \frac{8\alpha\omega_0(\alpha - i\omega)}{[(\alpha - i\omega)^2 + \omega_0^2]^2}, \quad (21)$$

where $\omega_0 = 2\pi \times 13$ kHz and $\alpha = 0.5\omega_0/\pi$. The attenuation is introduced through the complex velocity defined by

$$v(\omega) = v(\omega_{ref}) \left[1 + \frac{1}{\pi Q} \log\left(\frac{\omega}{\omega_{ref}}\right) - \frac{i}{2Q} \right], \quad (22)$$

where Q is the quality factor for either P-waves or S-waves, and v is either the P-wave velocity or S-wave velocity. The source-receiver separation is 3.048 m. Figure 2a is the seismogram calculated by the generalized R/T coefficients method, and Figure 2b is the result of Tubman et al. (1984). The comparison shows good agreement.

Boreholes with invaded zones

Next we choose two invaded zone models from Baker (1984) for comparison. There are two typical invaded zones. One is the damaged zone whose velocity is slower than the unperturbed formation velocity, and another is the flushed zone whose velocity is faster than the unperturbed formation velocity. The source function is a Ricker wavelet described by

$$F(\omega) = 4\sqrt{\pi} \frac{\omega^2}{\omega_0^3} \exp\left[-\left(\frac{\omega}{\omega_0}\right)^2\right], \quad (23)$$

where $\omega_0 = 2\pi \times 10$ kHz. There is no attenuation introduced in this example.

Figures 3 and 4 show the comparisons of the microseismograms calculated by the generalized R/T coefficients method with those calculated by the Thomson-Haskell method (Baker, 1984). The model parameters used to calculate the microseismograms in Figures 3 and 4 are given in Tables 2 and 3, respectively. The comparisons show excellent agreement.

Reflection caused by an outer-cylindrical formation

We now consider a scattering problem caused by an outer-cylindrical formation. The physical configuration of this model is shown in Figure 5(a) where a simple borehole is surrounded by a two-cylindrical-layer composite formation. Receivers are located at the borehole wall, and the source-receiver offset ranges from 10 m to 150 m. Other model parameters are listed in Table 4. This model is useful in the study of single-borehole imaging. The corresponding calculated seismograms are shown in Figure 5(b). To more clearly indicate the scattering phases (i.e., reflections from the interface between formation I and formation II), we normalized each trace by using its maximum value rather than a global scale for all traces. We can see from Figure 5(b) that phases show up as expected. In this calculation, the center frequency of the Ricker wavelet is 800 Hz, thus the corresponding characteristic wavelength is about 2 m to 3.5 m. The thickness of formation I is about 100 m and is much greater than the characteristic wavelength, therefore it is a typical high-frequency scattering problem. As mentioned earlier, the use of the normalized Hankel functions makes our algorithm stable numerically even for a very high-frequency model. We also tried this model with ordinary Hankel functions, but the calculation failed because of the arithmetic overflow.

EFFECTS OF INVADDED ZONES ON GEOMETRICAL SPREADING AND ATTENUATION ESTIMATION FOR P-WAVES

The geometrical spreading is a very important property of waves. When using amplitude decay to estimate intrinsic attenuation of the formation from waveform sonic logs, we must correct for the geometrical spreading of the wave. For a monopole source in a simple borehole, the geometrical spreading factor is $1/z$ for the P-wave (Roever et al., 1974; Winbow, 1980). With our efficient algorithm, we investigate the effect of complex invaded zones on the geometrical spreading and attenuation estimation for P-waves. The geometrical spreading

Table 1. Model parameters used for Figures 2a and 2b.

Layer	r (cm)	α (km/s)	β (km/s)	ρ (g/cm ³)	Q_p	Q_s
Fluid	4.7	1.68		1.2	20	
Casing	5.72	6.1	3.35	7.5	1000	1000
Cement	10.2	2.82	1.73	1.92	40	30
Formation	∞	4.88	2.6	2.16	60	60

factor, in general, is frequency-dependent (Paillet and Cheng, 1991; Quan et al., 1994). We assume an *apparent* geometrical spreading factor expressed by $1/z^p$ and determine the power p for the simple borehole and boreholes with invaded zones.

The magnitude of the recorded wave spectrum $A_{i+1}(f)$ at distance z_{i+1} from the source can be written in terms of $A_i(f)$ at distance z_i and geometrical spreading factor $1/z^p$ as

$$A_{i+1}(f) = \frac{A_i(f)z_i^p}{z_{i+1}^p} \exp\left[-\frac{\pi f}{Qv}(z_{i+1} - z_i)\right], \quad (24)$$

where f is frequency, v is velocity and $1/Q$ represents attenuation. Rearranging equation (24) and taking the logarithm, we obtain

$$p = \frac{1}{\log\left[\frac{z_{i+1}}{z_i}\right]} \left\{ \log\left[\frac{A_i(f)}{A_{i+1}(f)}\right] - \frac{1}{Q} \frac{\pi f(z_{i+1} - z_i)}{v} \right\} \quad (25)$$

We use equation (25) to estimate p from given model parameters and the synthetic seismograms calculated by the generalized R/T coefficients method.

Let us first consider a simple open borehole whose model parameters are shown in Figure 6a in which $Q_p = 40$. The

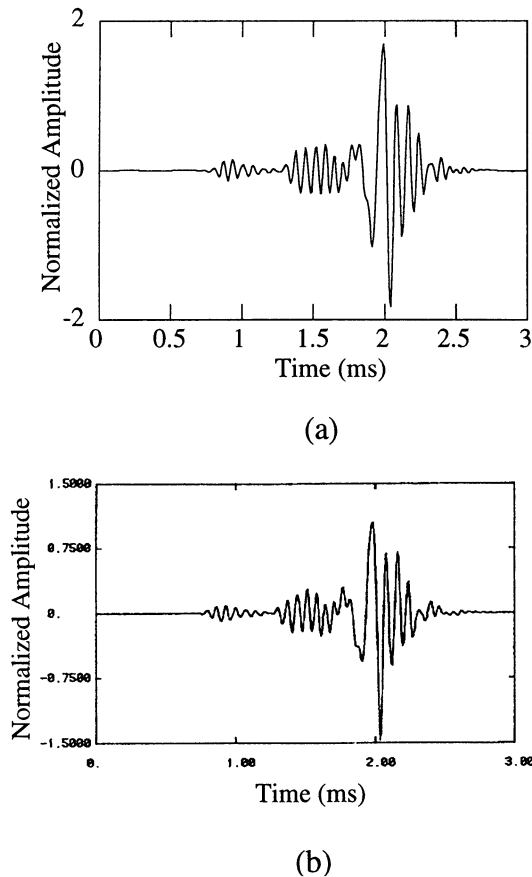


FIG. 2. (a) Seismogram calculated by the generalized R/T coefficients method for a four-layer cased borehole model. (b) Seismogram taken from Tubman (1984, 1055) for comparison with Figure 2a.

synthetic microseismograms in a common-source gather for this model are shown in Figure 6b. The source function used in this and later examples is given in equation (21) with $\omega_0 = 2\pi \times 14$ kHz and $a = 0.5\omega_0/\pi$. We use a short time window to extract the P-wave (first arrival) and perform FFT to obtain the spectrum $A_i(f)$. The peak spectrum amplitude $A_i(f_{peak})$ and the given model parameters are plugged into equation (25) to calculate the power p in the geometrical spreading factor $1/z^p$. For comparison, we change Q_p of the model to be 80 and 120, respectively, and calculate two more synthetic data sets. With these three common source gather data and multiple source-receiver pairs, we calculate several values of p 's by equation (25), and average these values to obtain the estimated power p in $1/z^p$. The estimated power of the geometrical spreading factor for this simple borehole model is $p = 1$, which is the same as was obtained in Roever et al. (1974) and Winbow (1980). For the purpose of reducing the effect of the window length and the contamination of later wavetrains, we

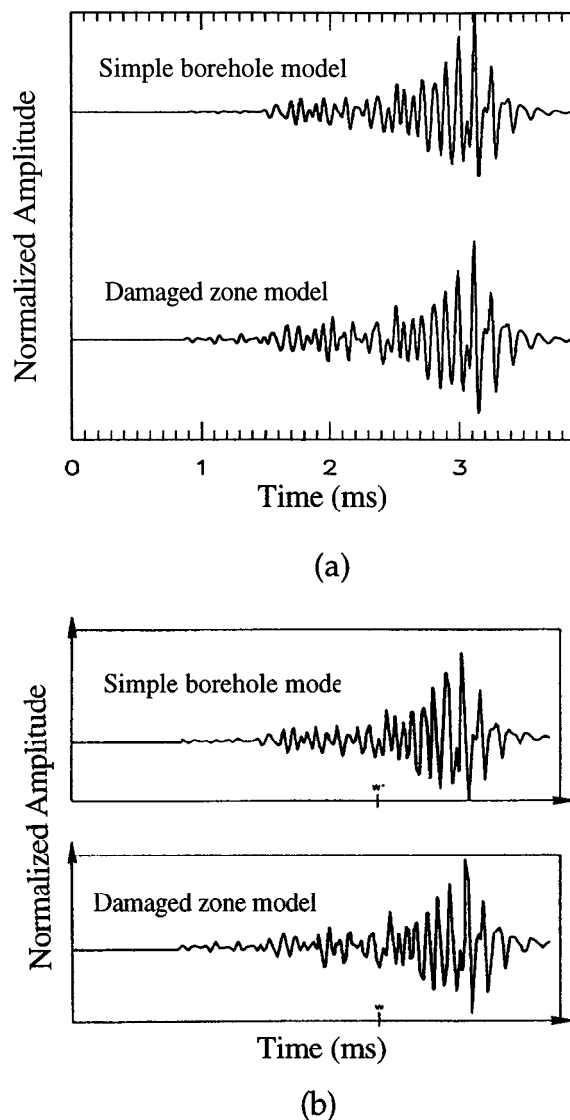


FIG. 3. (a) Seismograms calculated by R/T method for the models given in Table 2. (b) Seismograms taken from Baker (1984, Figure 7, 800) for comparison with Figure 3a.

use only the seismograms with source to receiver separation greater than 3.5 m for this and the later examples.

Figure 7a shows a model that consists of a fluid-filled borehole, a damaged zone, and an unperturbed formation. Since our modeling algorithm can efficiently handle an arbitrary number of radial layers, we use ten thin layers to model the invaded zone. In this model, Q_p is linearly changed from 35 to 40. Figure 7b is the microseismogram of a common source

gather calculated using this model. The invaded zone exhibits a significant effect on the wavetrains. The amplitude of the P-wave becomes relatively higher when the invaded zone is present. Because of the convergent effect of an increasing velocity zone (invaded zone) on the refracted wave (P-wave), the geometrical spreading is slower than that for a simple borehole. We also change Q_p of the invaded zone model to be 75-80, 115-120, respectively, and calculate two other synthetic data sets. Then, using equation (25) we obtain the estimated power of geometrical spreading $p = 0.5$ for this particular damaged zone model.

Another typical invaded zone is the flushed zone. Figure 8a shows this type of model. Figure 8b is the microseismogram of a common-source gather for this model in which $Q_p = 45-40$. Similarly, we calculate seismograms for $Q_p = 85-80$ and 125-120 as two other synthetic data sets. It is shown clearly that the geometrical spreading for this flushed zone model is greater than that for a simple borehole model because of the divergent effect of the decreasing velocity zone (flushed zone) on the refracted wave. The estimated power of the geometrical spreading factor is $p = 1.2$ for this particular flushed zone.

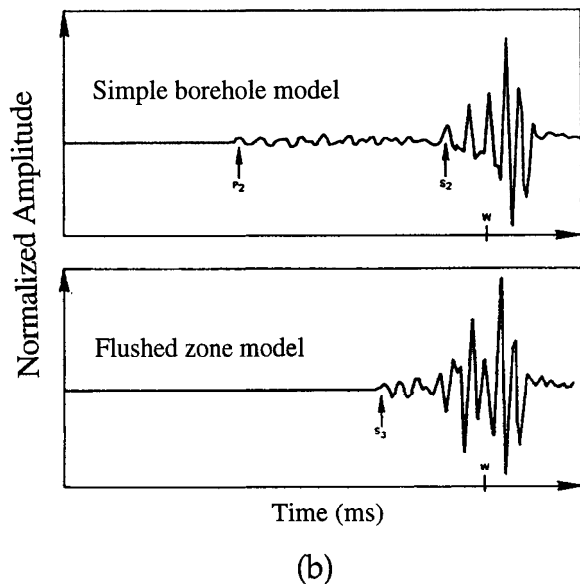
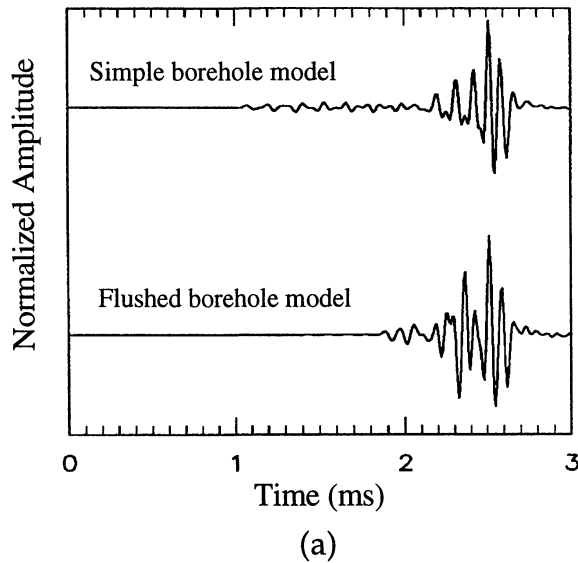


FIG. 4. (a) Seismograms calculated by R/T method for the models given in Table 3. (b) Seismograms taken from Baker (1984, Figure 10, 801) for comparison with Figure 4a.

Table 2a. Model parameters of a simple borehole.

Layer	r (cm)	α (km/s)	β (km/s)	ρ (g/cm ³)
Fluid	15.24	1.524		1.02
Formation	∞	4.876	2.743	2.25

Table 2b. Model parameters of a damaged borehole.

Layer	r (cm)	α (km/s)	β (km/s)	ρ (g/cm ³)
Fluid	15.24	1.524		1.02
Damaged zone	30.48	4.876	2.743	2.25
Formation	∞	5.364	2.895	2.25

Table 3a. Model parameters of a simple borehole.

Layer	r (cm)	α (km/s)	β (km/s)	ρ (g/cm ³)
Fluid	12.20	1.524		1.02
Formation	∞	3.962	1.828	2.14

Table 3b. Model parameters of a flushed borehole.

Layer	r (cm)	α (km/s)	β (km/s)	ρ (g/cm ³)
Fluid	12.20	1.524		1.02
Flushed zone	27.43	3.962	1.828	2.14
Formation	∞	3.048	2.133	1.734

Table 4. Parameters of a scattering model

Layer	r (m)	α (km/s)	β (km/s)	Q_p	Q_s	ρ (g/cm ³)
Fluid	0.11	1.6		3		1.0
Formation I	100	3.0	1.85	200	120	2.1
Formation II	∞	1.9	1.4	50	40	1.8

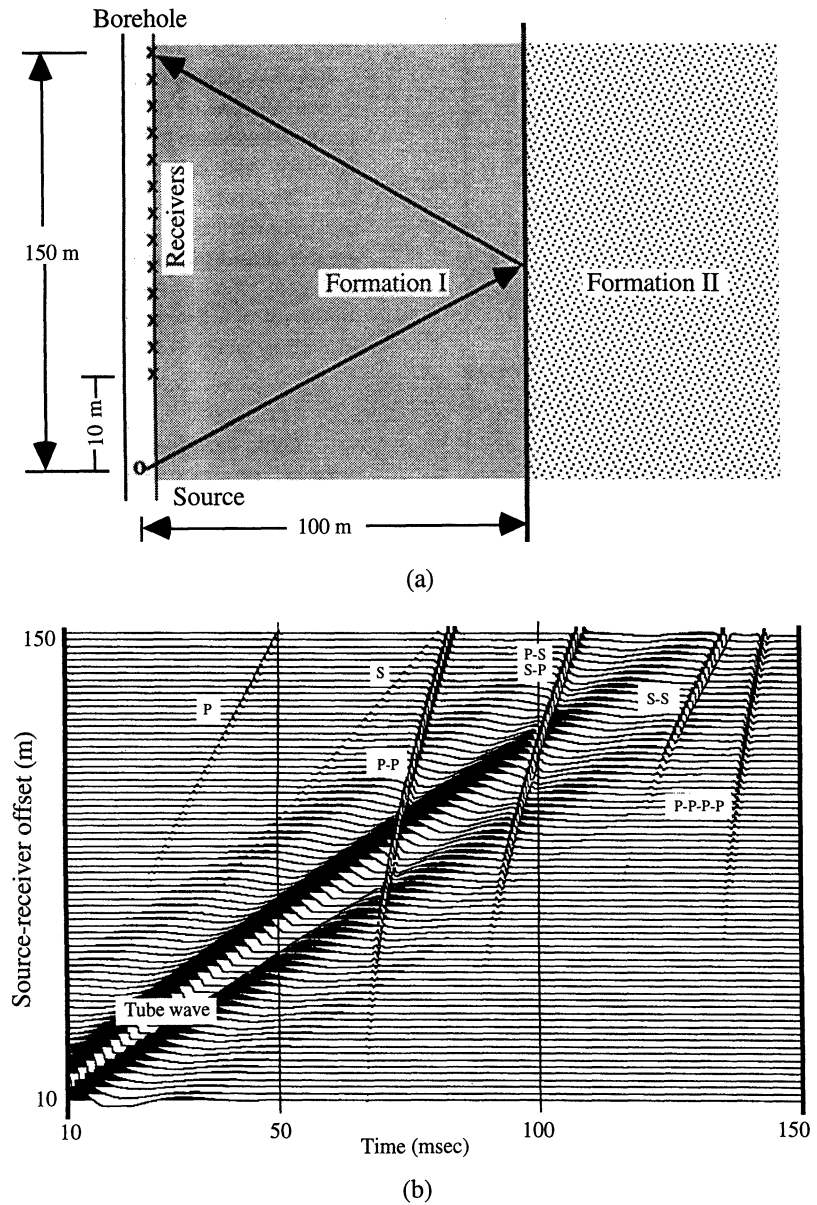


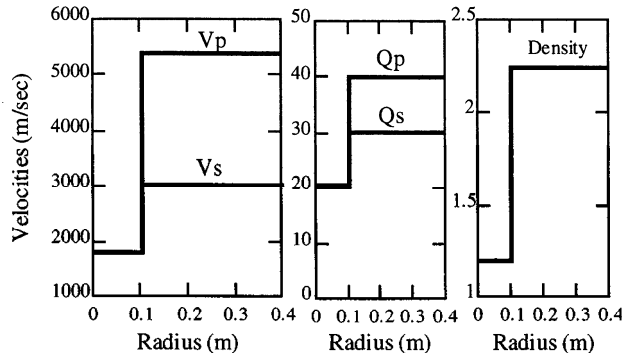
FIG. 5. (a) Configuration of the model. (b) Seismograms of horizontal displacement u . Here, "P" indicates the P head wave; "S" the direct S wave; " P - P , S - S , P - S , and S - P " are primary reflections; " P - P - P - P " is a P -wave multiple reflection.

The three different borehole models exhibit different geometrical spreading factors, $1/z^p$, for the P-wave. In summary, $p = 1$ for a simple borehole model $p < 1$ for a damaged zone model, and $p > 1$ for a flushed zone model.

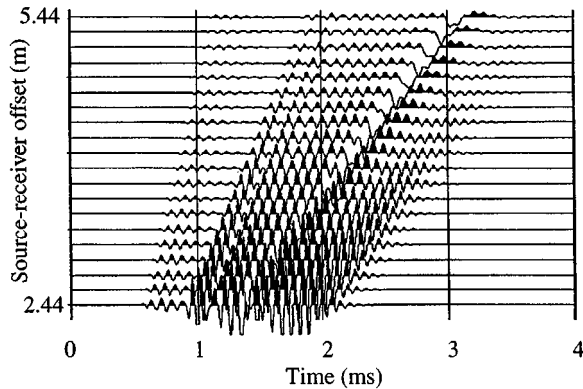
The amplitude decay method has been used to measure attenuation ($1/Q$) from acoustic logs (e.g., Cheng et al., 1982). Rearranging equation (24) and taking the logarithm, we obtain the following equation:

$$\frac{1}{Q} = \frac{v}{\pi f(z_{i+1} - z_i)} \log \left[\frac{A_i(f) z_i^p}{A_{i+1}(f) z_{i+1}^p} \right] \quad (26)$$

If the geometrical spreading factor $1/z^p$ is known, equation (26) can be used for attenuation estimation. All previous work used $p = 1$, which was obtained using the simple borehole model, for the geometrical spreading correction. From the study above, we know that the invaded zones have strong effects on geometrical spreading. To understand how the invaded zones effect the attenuation estimation based on equation (26), we compare the estimated Q_p values using the geometrical spreading correction $1/z$ with those using the correction $1/z^{0.5}$ for damaged zone model and the correction $1/z^{1.21}$ for flushed zone model. The peak spectrum amplitude $A_i (f_{peak})$ obtained from the microseismograms shown in Figures 6-8 are used again as data for equation (26) to estimate the P-wave attenuation Q_p . Tables 5-7 show the



(a)



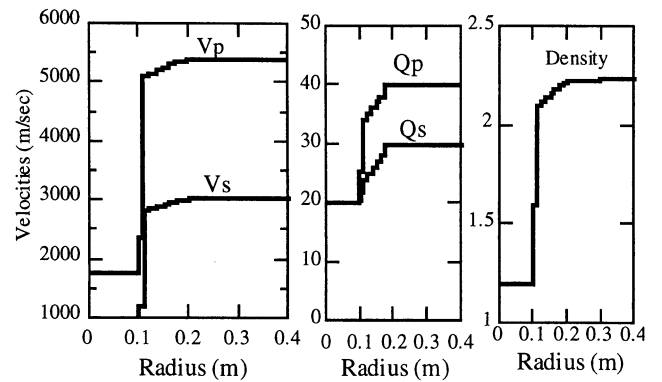
(b)

FIG. 6. (a) A simple borehole model; (b) Seismograms calculated for the simple borehole.

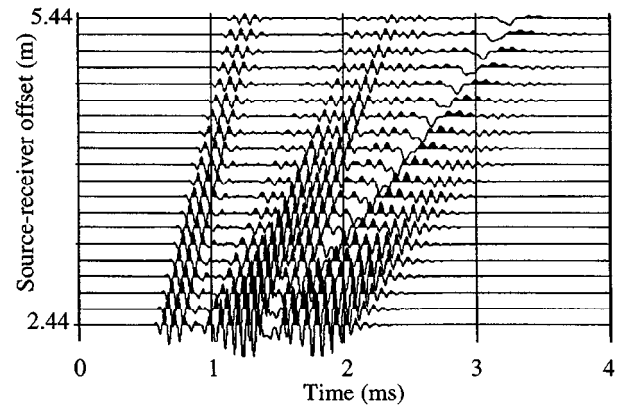
estimated results of Q_p values for the simple borehole model, damaged zone model, and the flushed zone model, respectively. It can be seen from Tables 5-7 that the estimation of attenuation using the amplitude decay method is very sensitive to the errors in geometrical spreading correction. This study reveals that for boreholes with invaded zones we may not simply use $1/z$ as the geometrical correction, though it is correct for the simple borehole, otherwise the attenuation could not be estimated correctly.

CONCLUSIONS

An approach based on generalized reflection and transmission coefficients is developed to calculate synthetic seismograms in radially layered media. The normalized Hankel functions and the recursive scheme are introduced to make the numerical procedure more efficient and stable. The validity of our new approach has been confirmed by comparing our results with the previous results available for a four-layer, cased-borehole model (Tubman et al., 1984) and for invaded zone models (Baker, 1984). As for applications of our new approach, we have investigated the effects of complex invaded



(a)



(b)

FIG. 7. (a) A damaged zone model. (b) Seismograms recorded in a borehole with a damaged zone. The amplitude of the P-wave decays significantly slower than that for the simple borehole, which indicates that the geometrical spreading effect is less than for a simple borehole.

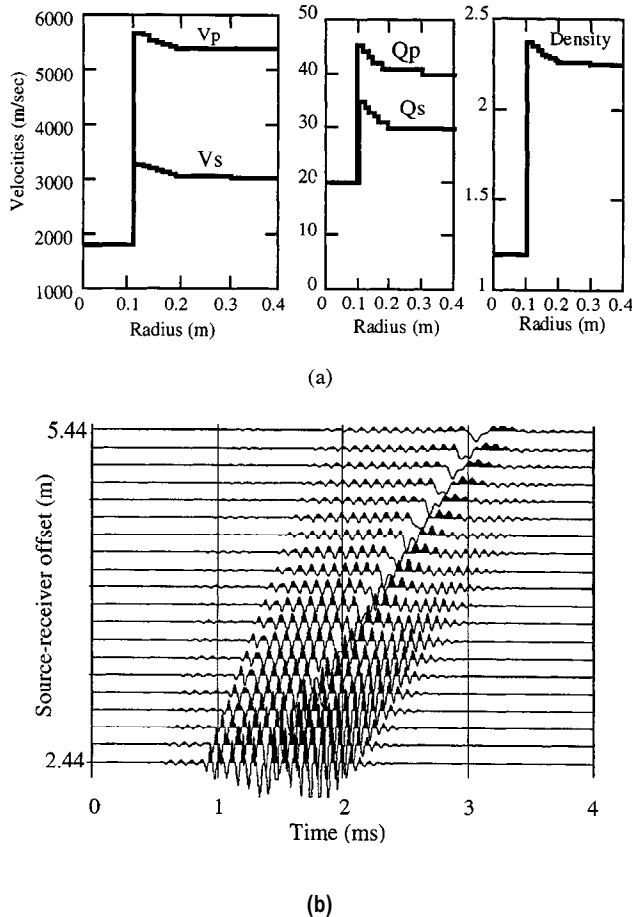


FIG. 8. (a) A flushed zone model; (b) Seismograms recorded in a borehole with a flushed zone. The amplitude of P-wave decays significantly faster than that for the simple borehole, which indicates that the geometrical spreading effect is greater than for a simple borehole.

zones on the geometrical spreading factor $1/z^p$ and the attenuation estimation for P-waves. We find that the power $p = 1$ for a simple borehole, $p < 1$ for a damaged zone model, and $p > 1$ for a flushed zone model. How large the power p deviates from 1 depends on the structure of the invaded zones, such as the velocity contrast and the invaded depth. For the specific borehole models investigated in this paper, $p = 0.5$ for the invaded zone model and $p = 1.2$ for the flushed zone model.

ACKNOWLEDGMENTS

We are grateful to former Assistant Editor James W. Rector III and two reviewers for their excellent reviews and suggestions. We wish to thank Drs. Drake S. Cameron and Sen T. Chen for stimulating discussion on the example of Figure 5. X. Chen acknowledges the support of the National Science Foun-

Table 5. Estimation of geometrical spreading $1/z^p$ and intrinsic attenuation $1/Q$ for the simple borehole.

Given Q_p	40	80	120
$1/z$	40	81	122

Table 6. Estimation of geometrical spreading $1/z^p$ and intrinsic attenuation $1/Q$ for the damaged zone model.

Given Q_p	35-40	75-80	115-120
$1/z^{0.5}$	90	<0	<0
$1/z$	39	80	129

Table 7. Estimation of geometrical spreading $1/z^p$ and intrinsic attenuation $1/Q$ for the flushed zone model.

Given Q_p	40	80	120
$1/z$	31	52	67
$1/z^{1.2}$	40	80	118

dation under EAR-9218923 and, in part, by the Department of Energy under grant DE-FG03-87ER13807. Y. Quan and J. M. Harris are grateful to the sponsors of the Seismic Tomography Project (STP) at Stanford University and DOE grant DE-FG03-95ER14535/A000 for supporting this work.

REFERENCES

- Baker, L. J., 1984, The effect of the invaded zone on the full wavetrain acoustic logging: *Geophysics*, 49, 789.
- Bouchon, M., and Aki, K., 1977, Discrete wavenumber presentation of seismic-source wavefields: *Bull. Seis. Soc. Am.*, 67, 259-277.
- Chen, X., 1993, A systematic and efficient method of computing normal modes for multilayered half-space: *Geophys. J. Internat.*, 115, 391-409.
- Cheng, C. H., Toksoz, M. N., and Willis, M. E., 1982, Determination of In-situ attenuation from full waveform acoustic logs: *J. Geophys. Res.*, 87, No. B7, 5477-5484.
- Kennett, B. L. N., 1983, *Seismic wave propagation in stratified media*: Cambridge Univ. Press.
- Luco, J. E., and Apsel, R. J., 1983, On the Green's function for a layered half-space, Part I: *Bull. Seis. Soc. Am.*, 73, 909-929.
- Paillet, L., and Cheng, C. H., 1991, *Acoustic waves in boreholes*: CRC Press, Inc.
- Quart, Y., Harris, J. M., and Chen, X. F., 1994, Acoustic attenuation logs using center frequency shift method: 64th Ann. Internat. Mtg., Soc. Expl. Geophys., Expanded Abstracts, 8-11.
- Roeber, W. L., Rosenbaum, J. H., and Vining, T. F., 1974, Acoustic waves from an impulsive source in a fluid-filled borehole: *J. Acoust. Soc. Am.*, 55, 1144-1157.
- Tubman, K. M., Cheng, C. H., and Toksöz, M. N., 1984, Synthetic full waveform acoustic logs in cased boreholes: *Geophysics*, 49, 1051-1059.
- Winbow, G. A., 1980, How to separate compressional and shear arrivals in a sonic log: 50th Ann. Internat. Mtg., Soc. Expl. Geophys., Expanded Abstracts, 16-20.
- Yao, Z., and Zheng, T., 1985, The generalized reflection-transmission coefficient method in acoustic well logging: *Acta Geophysica Sinica* (in Chinese), 28, 510-518.

APPENDIX

EXPLICIT EXPRESSIONS OF COEFFICIENT MATRIX

For $j > 1$ the explicit expressions of elements $\{e_{nm}^{(j)}\}$ defined in equation (7) are

$$\begin{aligned}
 e_{11}^{(j)} &= -v_{\alpha}^{(j)} \bar{H}_1^{(2)}(v_{\alpha}^{(j)} r) e^{iv_{\alpha}^{(j)}(r^{(j)}-r)}, \\
 e_{12}^{(j)} &= -ik \bar{H}_1^{(2)}(v_{\beta}^{(j)} r) e^{iv_{\beta}^{(j)}(r^{(j)}-r)}, \\
 e_{13}^{(j)} &= -v_{\alpha}^{(j)} \bar{H}_1^{(1)}(v_{\alpha}^{(j)} r) e^{iv_{\alpha}^{(j)}(r-r^{(j-1)})}, \\
 e_{14}^{(j)} &= -ik \bar{H}_1^{(1)}(v_{\beta}^{(j)} r) e^{iv_{\beta}^{(j)}(r-r^{(j-1)})}, \\
 e_{21}^{(j)} &= ik \bar{H}_0^{(2)}(v_{\alpha}^{(j)} r) e^{iv_{\alpha}^{(j)}(r^{(j)}-r)}, \\
 e_{22}^{(j)} &= v_{\beta}^{(j)} \bar{H}_0^{(2)}(v_{\beta}^{(j)} r) e^{iv_{\beta}^{(j)}(r^{(j)}-r)}, \\
 e_{23}^{(j)} &= ik \bar{H}_0^{(1)}(v_{\alpha}^{(j)} r) e^{iv_{\alpha}^{(j)}(r-r^{(j-1)})}, \\
 e_{24}^{(j)} &= v_{\beta}^{(j)} \bar{H}_0^{(1)}(v_{\beta}^{(j)} r) e^{iv_{\beta}^{(j)}(r-r^{(j-1)})}, \\
 e_{31}^{(j)} &= 2\mu^{(j)} [\Omega^{(j)} \bar{H}_0^{(2)}(v_{\alpha}^{(j)} r) + v_{\alpha}^{(j)} \bar{H}_1^{(2)}(v_{\alpha}^{(j)} r)/r] e^{iv_{\alpha}^{(j)}(r^{(j)}-r)}, \\
 e_{32}^{(j)} &= -ik \mu^{(j)} v_{\beta}^{(j)} [\bar{H}_0^{(2)}(v_{\beta}^{(j)} r) - \bar{H}_2^{(2)}(v_{\beta}^{(j)} r)] e^{iv_{\beta}^{(j)}(r^{(j)}-r)}, \\
 e_{33}^{(j)} &= 2\mu^{(j)} [\Omega^{(j)} \bar{H}_0^{(1)}(v_{\alpha}^{(j)} r) + v_{\alpha}^{(j)} \bar{H}_1^{(1)}(v_{\alpha}^{(j)} r)/r] e^{iv_{\alpha}^{(j)}(r-r^{(j-1)})},
 \end{aligned}$$

$$e_{34}^{(j)} = -ik \mu^{(j)} v_{\beta}^{(j)} [\bar{H}_0^{(1)}(v_{\beta}^{(j)} r) - \bar{H}_2^{(1)}(v_{\beta}^{(j)} r)] e^{iv_{\beta}^{(j)}(r-r^{(j-1)})},$$

$$e_{41}^{(j)} = -2ik \mu^{(j)} v_{\alpha}^{(j)} \bar{H}_1^{(2)}(v_{\alpha}^{(j)} r) e^{iv_{\alpha}^{(j)}(r^{(j)}-r)},$$

$$e_{42}^{(j)} = 2\mu^{(j)} \Omega^{(j)} \bar{H}_1^{(2)}(v_{\beta}^{(j)} r) e^{iv_{\beta}^{(j)}(r^{(j)}-r)},$$

$$e_{43}^{(j)} = -2ik \mu^{(j)} v_{\alpha}^{(j)} \bar{H}_1^{(1)}(v_{\alpha}^{(j)} r) e^{iv_{\alpha}^{(j)}(r-r^{(j-1)})},$$

$$e_{44}^{(j)} = 2\mu^{(j)} \Omega^{(j)} \bar{H}_1^{(1)}(v_{\beta}^{(j)} r) e^{iv_{\beta}^{(j)}(r-r^{(j-1)})},$$

where, $\Omega^{(j)} = k^2 - 1/2k_{\beta}^{(j)2}$ and $r^{(j-1)} < r < r^{(j)}$. For $j = 1$, the expressions of elements $\{e_{nm}^{(j)}\}$ defined in equation (8) are

$$e_{11}^{(1)} = -v_{\alpha}^{(1)} \bar{H}_1^{(2)}(v_{\alpha}^{(1)} r) e^{iv_{\alpha}^{(1)}(r^{(1)}-r)},$$

$$e_{12}^{(1)} = -v_{\alpha}^{(1)} \bar{H}_1^{(1)}(v_{\alpha}^{(1)} r) e^{iv_{\alpha}^{(1)} r},$$

$$e_{21}^{(1)} = -\lambda^{(1)} k_{\alpha}^{(1)2} \bar{H}_0^{(2)}(v_{\alpha}^{(1)} r) e^{iv_{\alpha}^{(1)}(r^{(1)}-r)},$$

$$e_{22}^{(1)} = -\lambda^{(1)} k_{\alpha}^{(1)2} \bar{H}_0^{(1)}(v_{\alpha}^{(1)} r) e^{iv_{\alpha}^{(1)} r},$$